J. Plasma Phys. (2024), *vol*. 90, 985900101
Published by Cambridge University Press
doi:10.1017/S0022377823001447

Development of the ambipolar electric field in a compressed current sheet and the impact on magnetic reconnection

Ami M. DuBois [1],†, **Chris Crabtree** [1] **and Gurudas Ganguli** [1]

[1]Plasma Physics Division, U.S. Naval Research Laboratory, Washington, DC 20375, USA

(Received 1 September 2023; revised 14 December 2023; accepted 15 December 2023)

Satellite data analysis of a compressed gyro-scale current sheet prior to magnetic reconnection in the magnetotail shows that electrostatic lower hybrid waves localized to the region of a transverse ambipolar electric field at the centre of the current sheet are driven by $\boldsymbol{E} \times \boldsymbol{B}$ velocity shear and result from compression. The presence and location of shear-driven waves around the centre of the current sheet, where the magnetic field reverses and the density gradient is minimal, is consistent with our model. This is notable because the free energy source is the curvature of the electron $\boldsymbol{E} \times \boldsymbol{B}$ flow and not the density gradient. Laboratory experiments and particle-in-cell (PIC) simulations have shown that shear-driven lower hybrid fluctuations are capable of producing anomalous cross-field transport (viscosity) and resistivity, which can trigger magnetic reconnection. We estimate the terms in the generalized Ohm's Law directly from MMS data as the spacecraft cross a gyro-scale current sheet. Our analysis shows that the wave effects (resistivity, diffusion and viscosity) and pressure anisotropy effects are comparable. We also find that the quasi-static electric field gradient is correlated with a non-gyrotropic electron distribution function, which is consistent with our model. Furthermore, theoretical arguments suggest agyrotropy is an indicator of the possibility for magnetic reconnection to occur.

Keywords: space plasma physics, plasma waves, plasma flows

1. Introduction

Current sheets are ubiquitous in space plasmas and are an important factor in how the Sun controls the near-Earth plasma environment (Chen 1993; Yamada, Kulsrud & Ji 2010; Petrukovich *et al.* 2015; Chen, Liu & Hu 2021; Chitta, Priest & Cheng 2021; Wilson *et al.* 2021). For example, during geomagnetically active periods, the solar wind compresses the magnetosphere creating ion-scale current sheets (Takahashi & Hones 1988; Schindler & Hesse 2008, 2010; Ganguli *et al.* 2020) in the magnetotail that have substructures embedded in the current density (McComas *et al.* 1986; Schindler & Birn 1993; Sergeev *et al.* 1993; Sanny *et al.* 1994; Hoshino *et al.* 1996; Sitnov, Guzdar & Swisdak 2003; Asano *et al.* 2004; Runov *et al.* 2004, 2006; Petrukovich *et al.* 2011; Norgren *et al.* 2018; DuBois *et al.* 2022). These gyro-scale current sheets are dominated by ambipolar effects that lead

† Email address for correspondence: ami.dubois@nrl.navy.mil

to unique physics such as multi-scale substructures and sheared $\boldsymbol{E} \times \boldsymbol{B}$ flows that have recently been observed (DuBois *et al.* 2022). Other features that are not captured in the Harris equilibrium (Harris 1962), such as unequal sheared flows in electrons and ions, intense electrostatic lower hybrid emissions in the centre of the current sheet where the density gradient is negligible, non-gyrotropic electron distribution functions, etc., are also observed in gyro-scale current sheets (DuBois *et al.* 2022). In this article, we attempt to explain the features observed in a gyro-scale current sheet prior to magnetic reconnection from *in situ* data using our kinetic current sheet model (Ganguli *et al.* 2020; DuBois *et al.* 2022) in which the ambipolar electric field is self-consistently generated at the gyro-scale by compression. We find that the global compression is the ultimate common physical origin for these seemingly unrelated observational features. Central to the phenomena is the generation of the perpendicular ambipolar electric field, which acts as a surrogate for the global compression.

1.1. *Origin of the ambipolar electric field*

As a current sheet is compressed to gyro-scale sizes, an effective charge imbalance arises in a non-uniform collisionless plasma due to the difference in the electron and ion gyro-radii ($\rho_{e,i}$), averaged over the plasma distribution. This generates a localized ambipolar electric field perpendicular to the magnetic field. The ambipolar electric field is a kinetic effect that can arise even for negligible electron pressure gradients, e.g. when density and temperature gradients are in opposite directions (Ganguli *et al.* 2020). Interestingly, the electron pressure gradient in the centre of gyro-scale magnetotail current sheets is often found to be flat (Runov *et al.* 2006), and yet this region is characterized by a localized electric field on the electron scale and consequently with sheared electron flow. This means that the electron flow is composed predominantly of $\boldsymbol{E} \times \boldsymbol{B}$ drift, with negligible diamagnetic drift. However, since the electric field is on a scale size smaller than the ion gyro-radius, the ions do not have a velocity equal to the $\boldsymbol{E} \times \boldsymbol{B}$ drift (Ganguli *et al.* 2020), and the ambipolar electric field must be balanced partially by a divergence in the ion stress tensor. This electric field renormalizes the gyro frequencies, making them shear dependent, and affects the particle orbits which separates the ion and electron scale physics through gyro averaging of the gradients. This leads to a current in the cross-field ('Hall') direction (Ganguli *et al.* 2020).

Historically, the Hall current forms in plasmas where a sufficiently large collision frequency renders the ions unmagnetized while leaving the electrons unaffected so that the electrons can $\boldsymbol{E} \times \boldsymbol{B}$ drift in the cross-field direction. This is a collisional effect, which can be large scale. In current sheet physics, 'Hall current' is often informally used to refer to any cross-field current, which is usually explained as a diamagnetic effect due to a pressure gradient, even in the collisionless magnetosphere. In a collisionless plasma, a cross-field current can also arise as a result of current sheet compression below an ion gyro-diameter, which can maintain a transverse electric field localized to electron scales in a nearly uniform quasi-neutral plasma (Ganguli, Lee & Palmadesso 1988*a*,*b*; Ganguli *et al.* 2020). This introduces novel kinetic features in the current sheet, including unequal and sheared $\boldsymbol{E} \times \boldsymbol{B}$ drifts because the gyro-averaged ion $\boldsymbol{E} \times \boldsymbol{B}$ drift is less than that of the electrons. The unequal drift causes a localized cross-field current resulting in a structured current density, and under certain conditions, the $\boldsymbol{E} \times \boldsymbol{B}$ shear-driven electron-ion hybrid (EIH) instability can generate waves in the lower hybrid frequency range (Ganguli *et al.* 1988*a*, 2020; Amatucci *et al.* 2003; DuBois *et al.* 2013).

The EIH instability is driven by the curvature of the cross-field flow and not the density gradient (Ganguli *et al.* 1988*a*), which makes it ideal for anomalous effects at the field reversal region where the density (pressure) gradient is found to be negligible.

https://doi.org/10.1017/S0022377823001447 Published online by Cambridge University Press

Additionally, experiments (DuBois *et al.* 2014) and simulations (Fletcher *et al.* 2019) show that the EIH instability can be the dominant source of emissions, even in the presence of a density gradient. The resulting turbulence affects the current sheet dynamics through anomalous resistivity, viscosity and cross-field diffusion. These inevitable gyro-scale current sheet phenomena have not been comprehensively studied but, based on recent studies (Ganguli *et al.* 2020; DuBois *et al.* 2022), could be quite consequential.

1.2. *Magnetic reconnection*

Reconnection can occur as a current sheet with a reversed magnetic field configuration is compressed (Schindler & Birn 1993; Nakamura *et al.* 2006; Sitnov *et al.* 2006; Schindler & Hesse 2008; Artemyev & Zelenyi 2013; Borovsky & Valdivia 2018; Artemyev *et al.* 2019). Simulations and theoretical treatments (Uzdensky, Loureiro & Schekochihin 2010; Daughton *et al.* 2011) envision that large-scale reorganization of the magnetotail could be a multi-scale process with forcing and feedback between reconnection at different sites. This indicates that the cumulative effect of reconnection at gyro-scale current sheets is important in a large-scale topological magnetic reorganization. Studies (Hwang *et al.* 2014; Xu *et al.* 2018) have suggested a possible connection between gyro-scale current sheets and reconnection, but the physics is still unclear. NASA's Magnetospheric Multiscale (MMS) mission (Burch *et al.* 2016) can resolve micro-scale features, so for the first time, it is possible to investigate gyro-scale current sheets in detail and assess their contributions to the generalized Ohm's Law and their role in magnetic reconnection.

Understanding how the frozen-in condition is broken to enable reconnection is an important open problem in space plasmas. Mechanisms include pressure anisotropy (Cai & Lee 1997; Le *et al.* 2009; Egedal, Le & Daughton 2013; Torbert *et al.* 2016*a*; Egedal *et al.* 2019; Greess *et al.* 2021), electron inertia (Sonnerup 1988; Valentini *et al.* 2007; Torbert *et al.* 2016*a*; Korovinskiy *et al.* 2021) and anomalous resistivity due to wave–particle interactions (Vaivads *et al.* 2004; Silin *et al.* 2005; Che 2017; Khotyaintsev *et al.* 2019). It has been found (Torbert *et al.* 2016*a*) that pressure and inertial terms may not be sufficient to balance the generalized Ohm's Law alone, and 3-D simulations showed enhanced fluctuations that imply waves may also play an important role in balancing the generalized Ohm's Law.

Lower hybrid waves have long been observed in current sheets and are postulated to be a potential source for anomalous resistivity. Generally, the density gradient driven lower-hybrid drift instability is cited as the source for lower hybrid waves at the centre of current sheets (Huba, Gladd & Papadopoulos 1978; Gurnett *et al.* 1979; Chen *et al.* 2020; Yoo *et al.* 2020). However, observations (Runov *et al.* 2006) show that the density gradient is negligible near the centre, which would require inward transport of lower hybrid waves that were generated away from the centre (Daughton 2003). It is not clear if this transport can be sustained in a strongly sheared magnetic field geometry formed when a guide field is present. We find that $\boldsymbol{E} \times \boldsymbol{B}$ velocity shear due to the perpendicular ambipolar electric field can naturally arise in the centre of current sheets around the magnetic reversal and can drive lower hybrid waves (DuBois *et al.* 2022). These waves, which in the absence of velocity shear reduce to the modified two stream instability for a non-zero wave vector along the magnetic field (Mcbride *et al.* 1972), are consistent with the local plasma conditions at the current sheet centre and require no extraordinary arguments to justify their existence. The importance of the perpendicular ambipolar electric field in compressed current sheets is further emphasized by particle-in-cell (PIC) simulations (Romero & Ganguli 1993) and laboratory experiments (Matsubara & Tanikawa 2000) that show shear-driven lower hybrid waves can contribute to substantial anomalous resistivity, viscosity and cross-field diffusion.

https://doi.org/10.1017/S0022377823001447 Published online by Cambridge University Press

Agyrotropy in the electron distribution function has been observed in gyro-scale current sheets (Lapenta *et al.* 2017; Chen *et al.* 2020). It has been argued that non-gyrotropic distributions are caused by meandering gyro orbits (Lapenta *et al.* 2017) or acceleration due to wave effects (Chen *et al.* 2020). When a guide field is present, as in the case discussed here, meandering orbits are absent. It is also unclear how heating due to wave–particle interactions driven by a local instability can create agyrotropy. However, it has recently been shown that strong agyrotropy can be generated by a localized perpendicular electric field with scale lengths less than an ion gyro-radius (i.e. ambipolar electric field) (Ganguli *et al.* 2018, 2020; DuBois *et al.* 2022). The formation of non-gyrotropic electron distribution functions has also been suggested to be an indicator of reconnection in both PIC simulations and *in situ* observations (Mahajan & Hazeltine 2000; Scudder & Daughton 2008).

This paper focuses on the importance of the perpendicular ambipolar electric field in a compressed, gyro-scale current sheet located in the Earth's magnetotail through MMS data analysis. Section 2 discusses the MMS data products and analysis techniques used in the study. Section 3 begins with a summary of previous results which characterize the current sheet, ambipolar electric field and $\boldsymbol{E} \times \boldsymbol{B}$ velocity shear-driven lower hybrid waves (§ 3.1). Section 3.2 discusses new calculations of the terms in the generalized Ohm's Law including the anomalous resistivity and viscosity due to wave turbulence with electrons and the off-diagonal pressure tensor terms. Section 4 concludes with a discussion of the impact on reconnection physics.

2. Data and methodology

The MMS mission comprises four identical spacecraft that fly in a pyramid-like formation to study kinetic-scale structures and dynamics in the electron diffusion region of thin and reconnecting current sheets. On July 3, 2017, the MMS spacecraft crossed a current sheet in the magnetotail at approximately 5:27:07 UTC. During this event, the MMS spacecraft were in the night side of Earth's plasma sheet on the dusk side of midnight, far from the magnetopause. We use high time resolution burst data from the fluxgate magnetometer (FGM) for magnetic field measurements (Russell *et al.* 2016), fast plasma investigation (FPI) for velocity, density, temperature, pressure tensor and distribution function measurements (Pollock *et al.* 2016), and from the FIELDS instrument (Torbert *et al.* 2016*b*) for electric field and electrostatic fluctuation measurements. The FGM burst measurements are at 128 Samples/s, the FIELDs burst measurements are at 8192 Samples/s, and the FPI burst measurements are at 6 Samples/s for ions and 33 Samples/s for electrons. All data are initially in the geocentric solar ecliptic (GSE) coordinate system.

Vector data are rotated from the GSE coordinate system into the local current sheet *LMN* coordinate system (figure 1) using the transformation matrix $[L,M,N] = [[-0.67, -0.68, -0.30], [-0.70, 0.71, -0.04], [-0.24, -0.18, 0.95]]$, where $\hat{L}$ is the outflow direction, $\hat{M}$ is the direction of the guide field and $\hat{N}$ is the direction normal to the current sheet. The transformation matrix is calculated from the minimum variance analysis (Denton *et al.* 2018). Details of the calculated transformation matrix can be found in the supplemental material of DuBois *et al.* (2022).

For the analysis in § 3, current sheet parameters such as velocity (V_{cs}) and width (L_{cs}) are important for determining if the current sheet is gyro-scale and for calculations of gradients. The reversal magnetic field (B_L) data from each spacecraft are shifted in time (dt) to minimize the difference between reversal times. The current sheet velocity is then estimated as $V_{cs} = \mathrm{d}N/\mathrm{d}t$, where d$N$ is the spacecraft distance from one another in $\hat{N}$.

https://doi.org/10.1017/S0022377823001447 Published online by Cambridge University Press

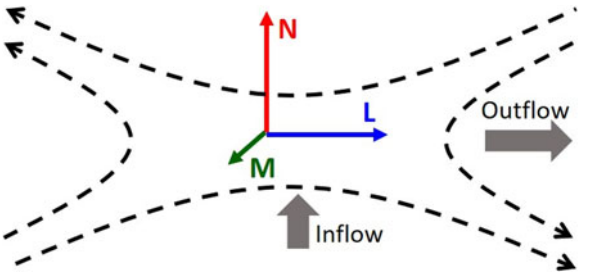

FIGURE 1. Local current sheet LMN coordinate system, where $\hat{L}$ is the outflow direction, $\hat{M}$ is the direction of the guide field and $\hat{N}$ is the direction normal to the current sheet.

Here, L_{cs} is estimated using the variance of B_L (Staniland *et al.* 2020). When B_L is steady, the variance is approximately 0, but when B_L diverges during a current sheet crossing, the variance is large. The beginning and ending times of the variance increase are used to identify the boundaries of the current sheet. Here, V_{cs} is used to convert the difference between the beginning/ending times to L_{cs}, which is normalized to ρ_i to show how the current sheet scale size compares with the ion-scale size. To smooth the data and infer dc level profiles of plasma parameters (figure 2), a boxcar average lowpass filter (∼3 Hz) is applied to the time series.

For the calculations of the terms in the generalized Ohm's Law (§ 3.2), the quantities are calculated from each MMS spacecraft individually. The average quantities (denoted by $\langle x \rangle$) are calculated from the boxcar average technique (above), and the fluctuation quantities (denoted by δx) are calculated by applying a lowpass filter with a cutoff frequency of 20 Hz to the raw data to filter out any high frequency noise and then subtracting the boxcar average. This ensures that only lower hybrid frequencies (3 to 20 Hz) are considered for the calculations of the terms in the generalized Ohm's Law, although including higher frequencies did not significantly affect the results discussed in § 3.2. We then account for time shifts between spacecraft using the same B_L shifting technique described above to get the dt between the reference spacecraft (MMS1) and the remaining spacecraft. The calculations from MMS2 and MMS3 spacecraft data are then shifted in time using the dt. Once the time shift is accounted for, the spacecraft data are averaged together.

3. Results and discussion

3.1. *Previous velocity shear-driven lower hybrid wave results*

The first evidence of velocity shear-driven lower hybrid waves in a compressed gyro-scale current sheet was previously reported by DuBois *et al.* (2022). The four MMS spacecraft traversed a gyro-scale current sheet of width $L_{cs} \sim 0.6\rho_i$ and crossed the magnetic reversal at approximately 5:27:07.02 UTC. DuBois *et al.* (2022, figure 1) shows a full summary of the plasma parameters in LMN coordinates for this event.

At the B_L reversal ($t = 7.02$ s), there is a guide field ($B_M \sim 10$ nT), and the magnetic field normal to the current sheet (B_N) is flat and near-zero inside the current sheet. The electric field normal to the current sheet (E_N) is the perpendicular ambipolar electric field (figure 2(*a*) – solid, blue) and has a scale length $\rho_e < L_E < \rho_i$, calculated from the half-width at half-max of E_N. A spectrogram of the E_N burst data reveals lower hybrid fluctuations (figure 2, left vertical axis), which are intense around the peak of the $V_{E\times B}$ flow. The ion velocity (V_i) is significantly smaller than the electron velocity (V_e), which indicates that the ions experience negligible electric field due to gyro averaging (Ganguli

https://doi.org/10.1017/S0022377823001447 Published online by Cambridge University Press

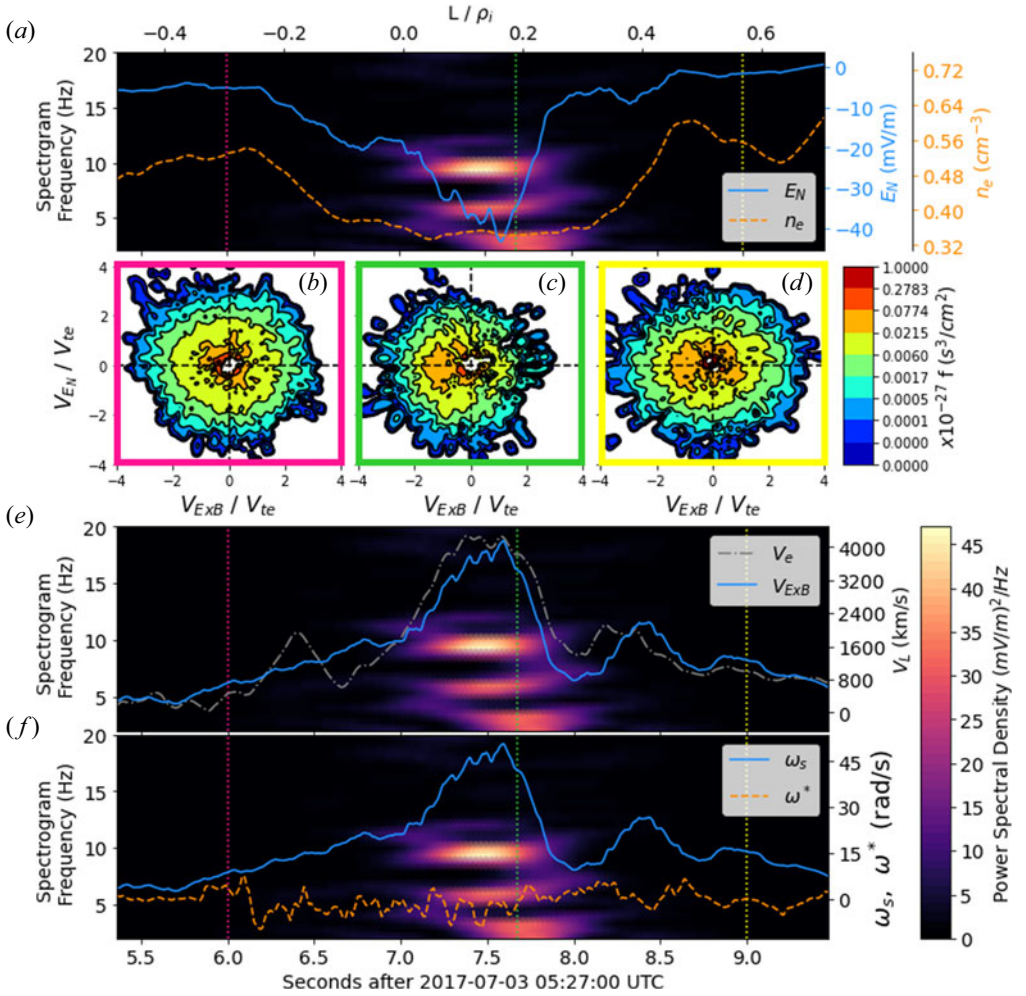

FIGURE 2. (*a*) E_N (solid, blue) and n_e (dash, orange), (*b*) the electron distribution function for $t = 6$ s (pink box), (*c*) $t = 7.67$ s (green box), (*d*) $t = 9$ s (yellow box), (*e*) V_e (dot-dash, grey) and $V_{E\times B}$ (solid, blue) in $\hat{L}$, and (*f*) ω_s (solid, blue) and ω^* (dash, orange) frequencies (right vertical axis). The spectrogram of electrostatic fluctuation power spectral density as a function of time is shown in panels (*a*,*e*,*f*). The top axis shows distance normalized to ρ_i. The vertical dotted lines indicate the times for which the electron distribution functions in panels (*b*–*d*) were calculated.

et al. 2020). The electron density (n_e) is nearly constant during the fluctuations (figure 2(*a*) – dashed, orange), which are localized around the field reversal region.

Non-gyrotropic distribution functions were observed in this event (Chen *et al.* 2020). Figure 2(*b*–*d*) shows the electron distribution functions calculated for $t = 6$ s (figure 2(*b*), pink), $t = 7.67$ s (figure 2(*c*), green) and $t = 9$ s (figure 2(*d*), yellow). The vertical dotted lines in figure 2(*a*,*e*,*f*) note the times of distribution functions. Figure 2(*c*) shows that the agyrotropy is correlated to the sheared perpendicular ambipolar electric field, while in figure 2(*b*,*d*), the electron distribution function is observed to be significantly less agyrotropic where the shear of the ambipolar electric field is reduced. This indicates that the agyrotropy is proportional to the shear of the electric field. This observation is supported by a kinetic model (Ganguli *et al.* 2020; DuBois *et al.* 2022), which establishes

https://doi.org/10.1017/S0022377823001447 Published online by Cambridge University Press

that the shear in the perpendicular ambipolar field is responsible for breaking the gyrotropy in the equilibrium distribution function, as opposed to the postulated wave heating (Chen *et al.* 2020).

The perpendicular ambipolar electric field breaks gyrotropy of the electron distribution function through the asymmetry in temperature in the gyro plane that arises due to the gradient in E_N included in the parameter $\eta(x) = 1 + (\mathrm{d}V_{E\times B}/\mathrm{d}x)/\Omega$, where the gradient of the $\boldsymbol{E}\times\boldsymbol{B}$ velocity, $\mathrm{d}V_{E\times B}/\mathrm{d}x$, is the velocity shear, and Ω is the cyclotron frequency (Ganguli *et al.* 2020). Increasing compression intensifies shear making $\mathrm{d}V_{E\times B}/\mathrm{d}x \rightarrow -\Omega$. Consequently, as $\eta \rightarrow 0$, the renormalized gyro frequency ($\Omega \rightarrow \sqrt{\eta}\Omega$) becomes vanishingly small and the gyro-radius becomes large representing the larger temperature, but the particles still gyrate around the magnetic field, albeit in non-circular orbits. For $\eta < 0$, the orbits are no longer simple gyration (Ganguli *et al.* 1988*b*) and the particles are effectively unmagnetized and accelerated by the electric field to high energies. This explains the origin of agyrotropy in the equilibrium distribution of compressed plasma layers and is notable because Scudder & Mozer (2005) found from data analysis that non-gyrotropic distribution functions could be generated by a quasi-static electric field, but the source of such an electric field was unknown. Theoretical arguments by Mahajan & Hazeltine (2000) and Scudder & Daughton (2008) suggest that the non-gyrotropic distribution function may be an indicator for imminent magnetic reconnection. Our data analysis confirms that non-gyrotropic distribution functions arise due to the localized perpendicular ambipolar electric field by their strong correlation. Physically, this is because the equilibrium electron $\boldsymbol{E}\times\boldsymbol{B}$ velocity is strongly sheared (DuBois *et al.* 2022), which makes the equilibrium electron $\eta_e \rightarrow 0$ and the ion $\eta_i < 0$. This configuration is unstable to EIH waves (discussed in § 1.1), which can heat the electrons and relax the velocity gradient resulting in a larger value of η_e in the saturated state. This demonstrates the critical role of the perpendicular ambipolar electric field, which may be considered as a surrogate for compression, and its importance to current sheet evolution. It can ultimately lead to reconnection (Scudder & Mozer 2005) if the electric field is sufficiently strong.

A large $\boldsymbol{E}\times\boldsymbol{B}$ velocity shear (figure 2(*e*) – solid, blue) in $\hat{L}(V_{E\times B-L})$ peaks with the wave activity. Here, $V_{E\times B-L}$ is nearly equal to the total electron flow (figure 2(*e*) – dashed, grey) in $\hat{L}$, V_{eL}, which indicates that the electrons are $\boldsymbol{E}\times\boldsymbol{B}$ drifting. It has been previously shown that velocity shear becomes important when $\omega_s/\omega_{LH} > 1$ (Romero & Ganguli 1993) and for this event, $\omega_s/\omega_{LH} \approx 8$. Additionally, the diamagnetic drift velocity $[\boldsymbol{V}_{\mathrm{drift}} = \nabla P_e \times \boldsymbol{B}/(n_e B^2)]$ in $\hat{L}$ is small in the region of the wave localization because $V_{eL} \approx V_{E\times B-L}$. The observed lower hybrid waves are characterized as shear-driven EIH waves because the diamagnetic drift frequency ($\omega^* = -k_\perp \boldsymbol{V}_{\mathrm{drift}}$ in figure 2(*f*) – dashed, orange, right vertical axis) is significantly smaller than the shear frequency ($\omega_s \sim \boldsymbol{V}_{E\times B}/L_E$ in figure 2(*f*) – solid, blue, right vertical axis). The wavenumber ($k_\perp$) in the calculation of the diamagnetic drift frequency can be estimated using a time shift method (Norgren *et al.* 2012). This rules out the density gradient as the driving mechanism (Romero & Ganguli 1993; DuBois *et al.* 2014, 2022; Ganguli *et al.* 2020). The observed waves also have a long wavelength with $k_\perp \rho_e \approx 0.18$ and $k_\perp L_E \approx 1$ indicating they are shear-driven lower hybrid fluctuations.

The current density, calculated from the moments data $[\boldsymbol{J} = e(n_i \boldsymbol{V}_i - n_e \boldsymbol{V}_e)]$, shows the electron current density (J_e) is dominant (figure 3(*a*) – solid, orange) because $V_i \ll V_e$ and it is comparable to the cross-field current, $J_{\mathrm{cf}} = en(\boldsymbol{E}\times\boldsymbol{B})$ (figure 3 – dot, purple). The large peak in J_{eL} (figure 3(*a*) – solid, orange) is localized to the region of E_N and the shear-driven lower hybrid waves, and the scale size is less than ρ_i. This indicates the formation of a gyro-scale current sheet. This is notable because previous studies

https://doi.org/10.1017/S0022377823001447 Published online by Cambridge University Press

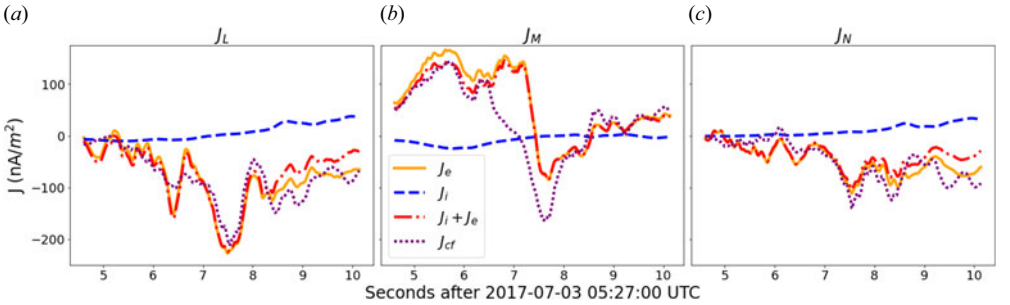

FIGURE 3. Current densities (*a*) J_L, (*b*) J_M and (*c*) J_N. The electron (orange, solid) and ion (blue, dashed) current densities are calculated from moments data. The total current density (red, dash-dot) is the sum of the electron and ion components. The cross-field current (purple, dot) is shown for comparison.

(Hwang *et al.* 2014; Xu *et al.* 2018) have shown a connection between current sheets with substructures in J and the onset of magnetic reconnection.

These previous results demonstrated that a localized perpendicular ambipolar electric field develops in a gyro-scale current sheet with scale size $L_{CS} < \rho_i$ and results in a sheared $\boldsymbol{E} \times \boldsymbol{B}$ velocity that drives lower hybrid fluctuations. Not only does this indicate a new mechanism to generate intense electrostatic turbulence near the magnetic field reversal, but these shear-driven lower hybrid waves can be used as a diagnostic to indicate if the system is in a path to magnetic reconnection since they imply the existence of a sheared electron flow and a non-gyrotropic electron distribution function, both of which may be prerequisites for magnetic reconnection (Mahajan & Hazeltine 2000; Scudder & Mozer 2005; Scudder & Daughton 2008). The shear-driven lower hybrid waves are also ideally localized in the current sheet centre and can contribute to anomalous dissipation, indicating they may play a significant role in magnetic reconnection (Romero & Ganguli 1993; Ganguli *et al.* 1994; Walker *et al.* 1997; Amatucci *et al.* 1998; Matsubara & Tanikawa 2000; Kumar, Mattoo & Jha 2002).

3.2. *Impact on magnetic reconnection*

One of the essential questions in reconnection physics is what effect breaks the frozen-in condition (where magnetic field lines move with the plasma)? One way for the frozen-in condition to be broken is through anomalous processes caused by the interaction of wave turbulence with electrons. Anomalous terms can be added to the generalized Ohm's Law,

$$\boldsymbol{E} + \boldsymbol{V}_e \times \boldsymbol{B} = \boldsymbol{\eta}_R \cdot \boldsymbol{J} + \boldsymbol{T} - \frac{1}{en_e}\nabla \cdot \bar{\boldsymbol{P}}_e + \frac{m_e}{e}\boldsymbol{V}_e \cdot \nabla \boldsymbol{V}_e, \tag{3.1}$$

where the first term on the right side of the equation ($\boldsymbol{\eta}_R \cdot \boldsymbol{J}$) is the anomalous resistivity (drag) due to the interaction of wave turbulence and electrons, the second term ($\boldsymbol{T}$) is the anomalous viscosity (momentum transport), the third term ($\nabla \cdot \bar{\boldsymbol{P}}_e$) is the electron pressure tensor, and the last term ($\boldsymbol{V}_e \cdot \nabla \boldsymbol{V}_e$) is the electron inertia. The anomalous terms can compete with other effects during the reconnection process. Due to measurement uncertainties, it is difficult to determine the dominance of any term unambiguously. For example, the magnitude of the anomalous terms depends on the wave amplitudes and is likely to change throughout the current sheet evolution due to the magnitude of

https://doi.org/10.1017/S0022377823001447 Published online by Cambridge University Press

compression. The time evolution of the pressure tensor term may also vary with current sheet evolution. Therefore, it is reasonable to account for all effects in determining the generalized Ohm's Law balance unless an unambiguous determination can be made for the dominance of a single process. In this section, we focus on estimating the anomalous, off-diagonal pressure tensor and electron inertia terms directly from MMS data in a gyro-scale current.

It was previously thought that density gradient driven lower hybrid drift waves could provide the anomalous resistivity necessary to trigger magnetic reconnection (Davidson & Gladd 1975; Silin *et al.* 2005). However, magnetotail observations and theoretical calculations now suggest that lower hybrid drift waves are unlikely to be the source because the waves are localized far from the magnetic field reversal region (Huba & Ganguli 1983) where magnetic reconnection is likely to be initiated, and the centre of current sheets are characterized by the lack of a density gradient (Runov *et al.* 2006), which is necessary to drive lower hybrid drift waves. Drake, Gladd & Huba (1981) argued that the lower hybrid drift instability may be supported at the centre due to a strongly varying magnetic field; but the model does not consider a guide field and the strong ambipolar electric field, which will also exist and intensify due to compression and substantially affect particle dynamics. One-dimensional PIC simulations by Birn, Schindler & Hesse (2004) that were initialized with a Harris equilibrium but were compressed by inflowing boundary conditions show the self-consistent formation of a transverse electric field, consistent with our kinetic model. In figure 2(*e*), we show that the net cross-field electron drift is close to the electron $\boldsymbol{E} \times \boldsymbol{B}$ drift, implying that the diamagnetic drift that is necessary to drive the lower hybrid drift instability is almost non-existent in the data. Two-dimensional simulations (Daughton 2003; Silin *et al.* 2005) showed that it may be possible for an electromagnetic lower hybrid drift wave to radiate inward to the centre if the current sheet is sufficiently thin. However, these simulations do not consider a realistic 3-D geometry in which the wave propagation characteristics may not convect the energy towards the centre. We find (DuBois *et al.* 2022) that the shear-driven EIH waves, which are ideally generated in the centre of the current sheet where magnetic reconnection is likely to be initiated, need no supplementary arguments to justify their presence in the centre of the current sheet. In addition, their predominant electrostatic nature ensures that they remain localized to the generation region to contribute robustly to anomalous dissipation.

Laboratory experiments (Matsubara & Tanikawa 2000; Kumar *et al.* 2002) have shown that the EIH instability can contribute to anomalous dissipation. The EIH anomalous resistivity estimated from PIC simulations by Romero & Ganguli (1993) showed that the sheared cross-field electron current is greatly reduced due to the growth of the EIH instability, indicating the presence of both anomalous resistivity and viscosity. It was also shown that the resistivity was proportional to the shear frequency, which is proportional to the global compression, thus implying that increasing compression may result in a larger anomalous resistivity and a faster reconnection rate. Additionally, theoretical arguments (Mahajan & Hazeltine 2000; Scudder & Daughton 2008) suggest that non-gyrotropic distribution functions are an indicator of the possibility for magnetic reconnection to occur, and the source of non-gyrotropic distribution functions is the localized ambipolar electric field (§ 3.1).

The anomalous resistivity ($\boldsymbol{\eta}_R$) due to the shear-driven EIH waves can be estimated directly from MMS data,

$$\boldsymbol{\eta}_R = 4\pi\, \boldsymbol{\nu}_\alpha / \omega_{pe}^2, \tag{3.2}$$

https://doi.org/10.1017/S0022377823001447 Published online by Cambridge University Press

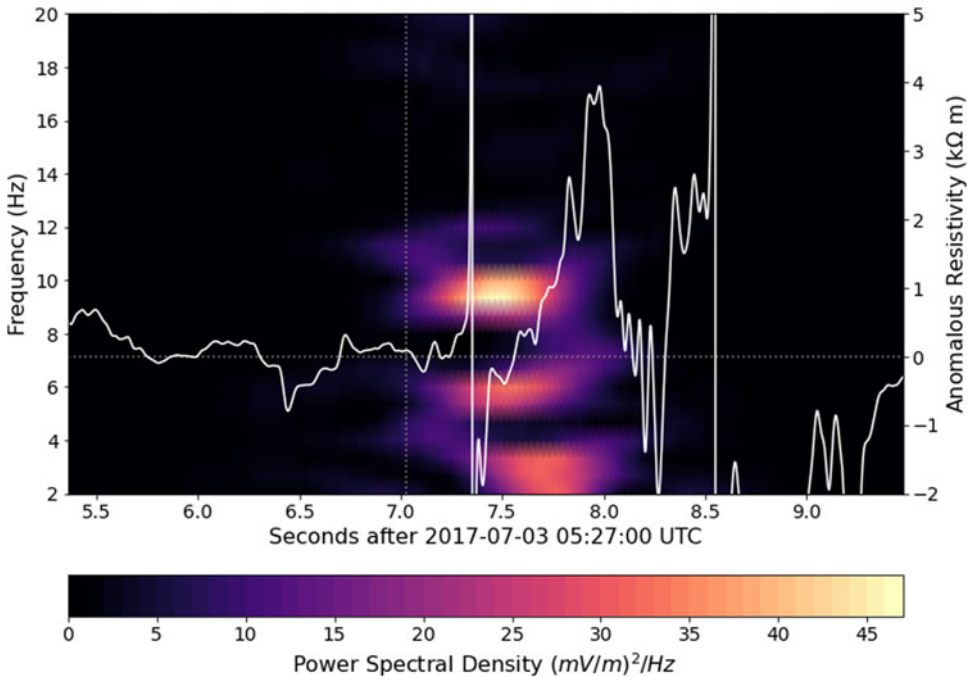

FIGURE 4. Anomalous resistivity in $\hat{M}$ (white) overlaid on spectrogram of lower hybrid fluctuations.

where, $\boldsymbol{\nu}_\alpha$ is the anomalous collision frequency,

$$\boldsymbol{\nu}_\alpha = e\langle \delta n_e \delta \boldsymbol{E} \rangle / \langle m_e n_e \boldsymbol{V}_e \rangle. \tag{3.3}$$

The electron density fluctuation quantity (δn_e) is calculated by taking the raw FPI qmoments burst data and subtracting the quasi-static profile (indicated by $\langle n_e \rangle$). The qmoments data products (Rager *et al.* 2018) are computed at one quarter of the 30 ms resolution time of the FPI moments burst data and have sufficient resolution for δn_e determination. The electric field fluctuation quantity ($\delta \boldsymbol{E}$) can be similarly calculated using the electric field burst data. The anomalous resistivity in $\hat{M}(\eta_{RM})$ is the resistivity in the reconnection direction of the current sheet. Figure 4 shows η_{RM} calculated from δE_M and δn_e using the methodology described in § 2, overlaid on the spectrogram of shear-driven lower hybrid waves. The anomalous resistivity is relatively constant in the time prior to the fluctuations, and then begins to quickly increase during the time of the shear-driven EIH waves. The anomalous resistivity due to the interaction between shear-driven lower hybrid wave turbulence and electrons is estimated to have a peak value of $\eta_{RM} = 4 \pm 2.9$ kΩ m. This is similar to what Silin *et al.* (2005) estimated using spacecraft potential to infer the electron density for lower hybrid fluctuations observed in Cluster data. The anomalous resistivity term in the generalized Ohm's Law can be calculated using η_{RM} and the current density, J_M (figure 3(*b*) – dash-dot, red). Figure 5(*a*) shows that the anomalous resistivity term (solid, white) is nearly 0 prior to the shear-driven lower hybrid waves and then, during the time of the waves, begins to decrease and has a minimum value of $(\eta_R J)_M = -0.18 \pm 0.12$ mV m^{-1}.

It has also been shown that the anomalous viscosity ($\boldsymbol{T}$) associated with lower hybrid waves can be calculated directly from MMS data (Graham *et al.* 2022). To estimate the

https://doi.org/10.1017/S0022377823001447 Published online by Cambridge University Press

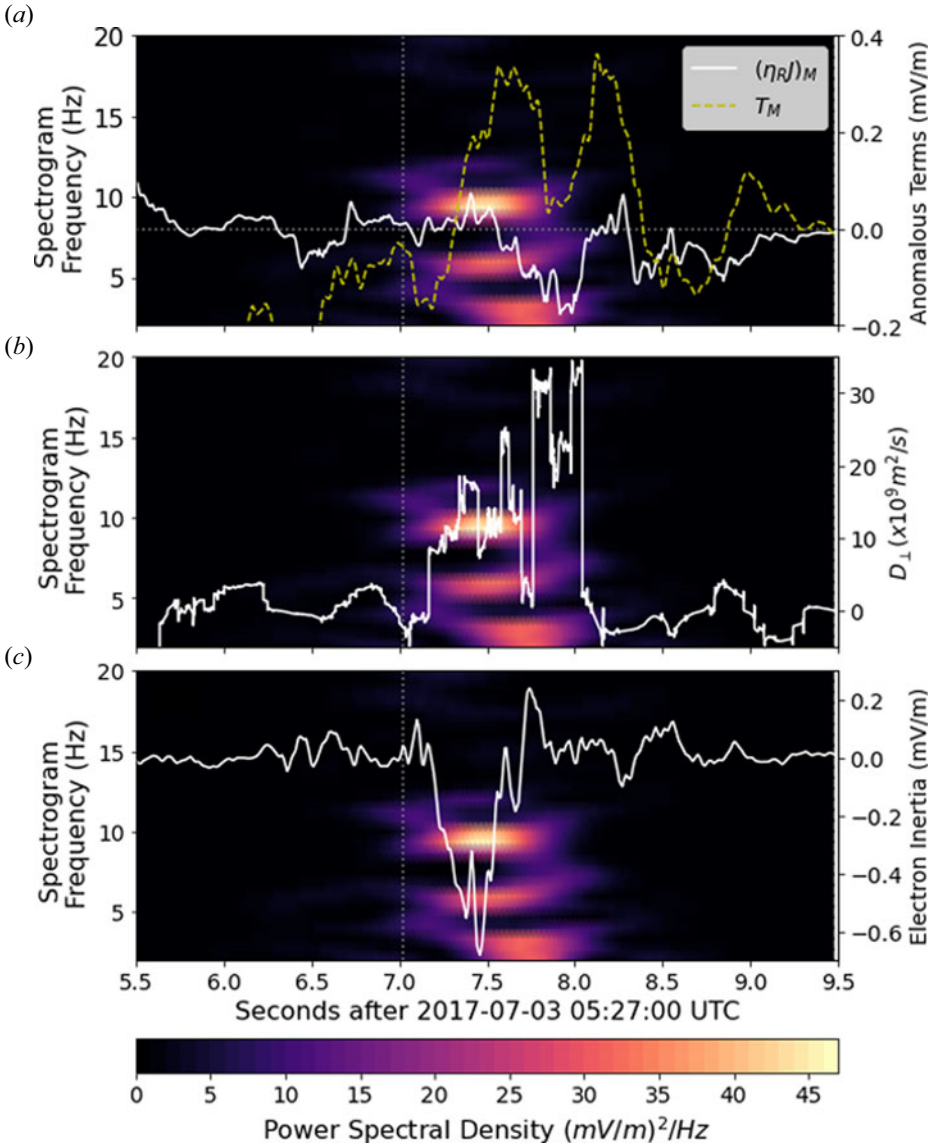

FIGURE 5. (*a*) Anomalous resistivity term $(\eta_R J)_M$ (solid, white) and anomalous viscosity term T (yellow, dashed) estimated from data. (*b*) Cross-field diffusion coefficient (solid, white). (*c*) Electron inertial term (solid, white). Plots are overlaid on the spectrogram of lower hybrid fluctuations (left vertical axis).

anomalous viscosity in $\hat{M}$, we use

$$T_M = \langle \delta V_L \delta B_N \rangle - \langle \delta V_N \delta B_L \rangle + \left[\frac{\langle \delta n_e \delta V_L \rangle \langle B_N \rangle + \langle \delta n_e \delta B_N \rangle \langle V_L \rangle - \langle \delta n_e \delta V_N \rangle \langle B_L \rangle - \langle \delta n_e \delta B_L \rangle \langle V_N \rangle}{\langle n_e \rangle} \right], \quad (3.4)$$

where δV is the fluctuation quantity of the electron flow (subscript indicates direction in LMN), δB is the fluctuation quantity of the magnetic field and $\langle \delta V \delta B \rangle$ is calculated

https://doi.org/10.1017/S0022377823001447 Published online by Cambridge University Press

by multiplying the fluctuation quantities together, followed by calculating the boxcar average. Figure 5(*a*) shows the anomalous viscosity in $\hat{M}$ estimated directly from MMS data (dashed, yellow). The anomalous viscosity begins to increase during the time of the shear-driven lower hybrid waves, remains localized to the region of the waves and has a peak value of $T_M = 0.43 \pm 0.28$ mV m^{-1}, and is in the opposite direction of the anomalous resistivity.

The cross-field diffusion coefficient ($D_\perp$), which is related to anomalous viscosity, can be estimated directly from MMS data using

$$D_\perp = -\frac{\langle \delta n_e \delta V_N \rangle}{\nabla \langle n_e \rangle_N}, \tag{3.5}$$

where the density gradient is taken in $\hat{N}$ or the direction of motion of the spacecraft across the current sheet. The cross-field diffusion coefficient is shown in figure 5(*b*), where there is a large increase as soon as shear-driven lower hybrid waves are observed and then quickly decreases back to near-zero as the shear-driven waves disappear. This sudden increase in the cross-field diffusion indicates anomalous electron drift and diffusion across the current sheet, which can modify the reconnection process. This was similarly observed in laboratory experiments (Matsubara & Tanikawa 2000).

The electron inertia term in $\hat{M}(I_{eM})$ can also be calculated directly from the MMS data (figure 5*c*) using

$$I_{eM} = \frac{m_e}{e}(\boldsymbol{V_e} \cdot \nabla)\boldsymbol{V_e} = \frac{m_e V_{eN}}{e}\frac{\mathrm{d}V_{eM}}{\mathrm{d}N}, \tag{3.6}$$

where, again, the gradient is taken in $\hat{N}$ because this is the direction of motion of the spacecraft across the current sheet, and V_{eN} and V_{eM} are boxcar averaged (quasi-static) electron velocities. The electron inertial term peaks at -0.7 ± 0.15 mV m^{-1} during the time of the intense ambipolar electric field and is comparable to the other terms in the generalized Ohm's Law. As we have already shown, the majority of the electron flow consists of the $\boldsymbol{E} \times \boldsymbol{B}$ velocity. Since the $\boldsymbol{E} \times \boldsymbol{B}$ velocity also has a component in $\hat{M}$, the quasi-static electron velocities are related to the quasi-static ambipolar electric field. This shows how the ambipolar effect can enhance the inertial term, which is typically considered to be less important and usually ignored in estimates of the generalized Ohm's Law balance.

A previous study (Egedal *et al.* 2019) of MMS data has shown that the off-diagonal pressure tensor can be responsible for breaking the frozen-in condition, but significant lower hybrid fluctuations were not detected in the reconnecting current sheet. Another study (Torbert *et al.* 2016*a*) has shown that the pressure and inertial terms may not actually be sufficient to balance the generalized Ohm's Law. We calculate the off-diagonal pressure tensor terms in $\hat{M}$ from MMS moments data using

$$\frac{1}{en_e}(\nabla \cdot \bar{\boldsymbol{P}}_{\boldsymbol{e}})_M = \frac{1}{en_e}\left(\frac{\mathrm{d}P_{LM}}{\mathrm{d}L} + \frac{\mathrm{d}P_{MN}}{\mathrm{d}N}\right). \tag{3.7}$$

The pressure tensor terms depend on gradients in $\hat{L}$ and $\hat{N}$, assuming $\partial/\partial M \sim 0$ (Egedal *et al.* 2019). Figures 6(*a*) and 6(*b*) show the pressure terms, P_{LM} and P_{MN}, respectively, for each spacecraft. The signals have been shifted in time using the method described in § 2. There are several methods that can be used to calculate the gradients of the two terms in (3.7). First, if the spacecraft are moving across the current sheet in the same direction of the gradient, then one can take the direct gradient of the pressure by converting time

https://doi.org/10.1017/S0022377823001447 Published online by Cambridge University Press

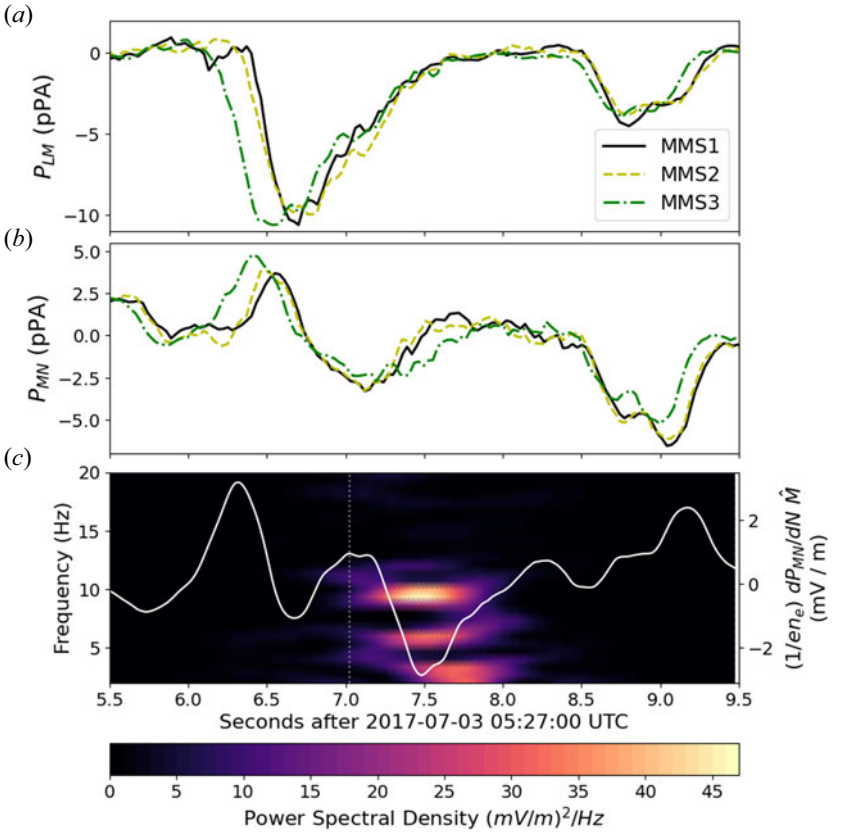

FIGURE 6. Off-diagonal pressure tensor terms (*a*) P_{LM} and (*b*) P_{MN} measured by MMS1 (solid, black), MMS2 (dashed, yellow) and MMS3 (dash-dot, green). (*c*) Resulting pressure tensor gradient estimated from P_{MN} data (solid, white) overlaid on the spectrogram of shear-driven lower hybrid fluctuations.

to distance using the current sheet velocity. If there is a steady increase or decrease in the signals with no variations between the spacecraft signals, and the spacecraft motion is in the same direction as the gradient, then the gradient can also be calculated using $(\max - \min)/(x_{\max} - x_{\min})$, where $x_{\max}$ is the position of the spacecraft in the gradient direction when the signal is the maximum point and $x_{\min}$ is the position of the spacecraft in the gradient direction when the signal is at the minimum point. A more straightforward method depends on if there are variations in the signals for each spacecraft and can be used regardless of whether the spacecraft direction and the gradient direction are the same.

For our case of interest, the spacecraft are moving across the current sheet in $\hat{N}$, making the second term in (3.7) straightforward to calculate using the third method. Figure 6(*b*) illustrates that during the time of the shear-driven lower hybrid waves, the MMS1 (solid, black) and MMS2 (dashed, yellow) measure relatively the same signal, while MMS3 (dash dot, green) is noticeably different. Therefore, the gradient can be calculated using $(P_{MN1} - P_{MN3})/(N_1 - N_3)$. This calculation can likewise be completed using MMS2 and MMS3 data, and then the average can be taken. The first term in (3.7) requires taking the gradient with respect to $\hat{L}$, which means only the third method is applicable to this calculation since spacecraft motion across the current sheet is in $\hat{N}$. Looking at figure 6(*a*), the P_{LM}

https://doi.org/10.1017/S0022377823001447 Published online by Cambridge University Press

data have no variations between spacecraft during the region of interest (between 7 and 8 seconds). Therefore, the gradient of the P_{LM} term in (3.7) cannot be estimated directly from the data. The pressure tensor gradient is therefore estimated using only the P_{MN} term (figure 6*c*). There is a peak of approximately -2.8 ± 4.5 mV m^{-1} in the pressure tensor gradient during the time of the shear-driven lower hybrid fluctuations.

Interestingly, the related off-diagonal terms in the pressure tensor can be generated due to compression in a 2-D magnetic field, as was shown in studies of dipolarization fronts by Ganguli *et al.* (2018, 2020). In a 2-D magnetic field, compression creates the 2-D ambipolar potential, $\Phi(x, z)$, which generates $E_{\parallel} \propto \partial\Phi/\partial z$ along the magnetic field line. Pressure anisotropy must arise to balance the $E_{\parallel}$ in a collisionless plasma. This indicates that the off-diagonal pressure tensor terms may be related to the ambipolar electric field through compression.

4. Conclusions

In situ measurements show that a localized perpendicular ambipolar electric field develops in a gyro-scale current sheet as it is compressed to a scale size of $L_{cs} < 2\rho_i$. This perpendicular ambipolar electric field results in a strong electron sheared $\boldsymbol{E} \times \boldsymbol{B}$ velocity, which drives electrostatic lower hybrid fluctuations. A non-gyrotropic electron distribution function is observed and is shown to be generated by the shear in the perpendicular ambipolar electric field. This is noteworthy because it has been previously suggested that the presence of non-gyrotropic electron distribution functions may be a precursor to magnetic reconnection occurring. The sheared flow and non-gyrotropic electron distribution function observed in the current sheet cannot be described using the Harris equilibrium.

The terms in generalized Ohm's Law can be estimated directly from the data. During the time of shear-driven lower hybrid waves, the cross-field diffusion increases rapidly from approximately 0 to $(30 \pm 12) \times 10^9$ m^2 s^{-1} and decreases back to near-zero as the shear-driven lower hybrid waves disappear. The cross-field diffusion relates the particle flow and the fluctuations in $\hat{N}$. So, this rapid increase and decrease around the time of the shear-driven lower hybrid waves indicates that the waves can modify the reconnection process through the diffusion of momentum across the current sheet. The data also show that the wave-induced effects (anomalous resistivity and viscosity), pressure anisotropy effects and electron inertia peak during the time of the shear-driven lower hybrid fluctuations, and we find that all terms are comparable at the moment of the measurement. Therefore, the roles of the anomalous resistivity, viscosity, pressure tensor and electron inertia terms should be equally treated in determining the balance in the generalized Ohm's Law and the breaking of the frozen-in condition. It is noted that the relative influence of the different terms in the generalized Ohm's Law will very likely change as time proceeds, and the current sheet becomes more compressed and closer to reconnection. In future work, a statistical study of gyro-scale current sheets of different thicknesses will be conducted to compare how the terms in generalized Ohm's Law evolve and if certain terms become more significant than others.

These results are significant because they stress the importance of the perpendicular ambipolar electric field, which is the surrogate of global compression, in the current sheet physics and its impact on the reconnection process. The perpendicular ambipolar electric field can act as a free energy source to drive electrostatic lower hybrid fluctuations, which can provide anomalous resistivity and viscosity. It has also been suggested that the off-diagonal pressure tensor terms may be related to the ambipolar electric field through compression. This, and the fact that all terms were found to be comparable, indicate

https://doi.org/10.1017/S0022377823001447 Published online by Cambridge University Press

that multiple processes may be necessary to trigger magnetic reconnection. Therefore, breaking the frozen-in condition depends on the kinetic-scale features and dynamics occurring within gyro-scale current sheets.

In a forthcoming article (Crabtree *et al.* 2024), we generalize our model to 2-D and formally show that the primary driver of physics in the current sheet is the global compression. The compression results in thinning of the current sheet, which generates the highly inhomogeneous transverse ambipolar electric field when sufficiently thin. This, in turn, leads to velocity shear-driven phenomena and also introduces anisotropy in the pressure tensor, both of which affect the balance of the generalized Ohm's Law. The intensity of these phenomena is proportional to the scale size of the current sheet and hence to the intensity of the compression.

Acknowledgements

All MMS data used in this manuscript are publicly available and can be found online at the MMS Science Data Center. This work was supported by the Naval Research Laboratory Base Program.

Editor Troy Carter thanks the referees for their advice in evaluating this article.

Declaration of interests

The authors report no conflict of interest.

REFERENCES

Amatucci, W.E., Ganguli, G., Walker, D.N., Gatling, G., Balkey, M.M. & McCulloch, T. 2003 Laboratory investigation of boundary layer processes due to strong spatial inhomogeneity. *Phys. Plasmas* **10** (5), 1963.

Amatucci, W.E., Walker, D.N., Ganguli, G., Duncan, D., Antoniades, J.A., Bowles, J.H., Gavrishchaka, V. & Koepke, M.E. 1998 Velocity-shear-driven ion-cyclotron waves and associated transverse ion heating. *J. Geophys. Res.* **103** (A6), 11711–11724.

Artemyev, A.V., Angelopoulos, V., Runov, A. & Petrukovich, A.A. 2019 Global view of current sheet thinning: plasma pressure gradients and large-scale currents. *J. Geophys. Res.: Space Phys.* **124** (1), 264–278.

Artemyev, A. & Zelenyi, L. 2013 Kinetic structure of current sheets in the earth magnetotail. *Space Sci. Rev.* **178**, 419–440.

Asano, Y., Mukai, T., Hoshino, M., Saito, Y., Hayakawa, H. & Nagai, T. 2004 Current sheet structure around the near-Earth neutral line observed by Geotail. *J. Geophys. Res.: Space Phys.* **109** (A02212), 1–18.

Birn, J., Schindler, K. & Hesse, M. 2004 Thin electron current sheets and their relation to auroral potentials. *J. Geophys. Res.* **109**, A02217.

Borovsky, J.E. & Valdivia, J.A. 2018 The Earth's magnetosphere: a systems science overview and assessment. In *Surveys in Geophysics*, vol. 39. Springer.

Burch, J.L., Moore, T.E., Torbert, R.B. & Giles, B.L. 2016 Magnetospheric multiscale overview and science objectives. *Space Sci. Rev.* **199**, 5–21.

Cai, H.J. & Lee, L.C. 1997 The generalized Ohm's law in collisionless magnetic reconnection. *Phys. Plasmas* **4** (3), 509–520.

Che, H. 2017 How anomalous resistivity accelerates magnetic reconnection. *Phys. Plasmas* **24** (8), 082115.

Chen, J. 1993 Physics of the magnetotail current sheet. *Phys. Fluids* B **5** (7), 2663–2670.

Chen, C., Liu, Y.D. & Hu, H. 2021 Macro magnetic holes caused by ripples in heliospheric current sheet from coordinated imaging and parker solar probe observations. *Astrophys. J.* **921** (15), 1–10.

Chen, L.-J., Wang, S., Le Contel, O., Rager, A., Hesse, M., Drake, J., Dorelli, J., Ng, J., Bessho, N., Graham, D., *et al.* 2020 Lower-hybrid drift waves driving electron nongyrotropic heating and vortical flows in a magnetic reconnection layer. *Phys. Rev. Lett*. **125**, 025103.

Chitta, L.P., Priest, E.R. & Cheng, X. 2021 From formation to disruption: observing the multiphase evolution of a solar flare current sheet. *Astrophys. J*. **911** (133), 1–12.

Crabtree, C., Ganguli, G., DuBois, A.M. & Sen, A. 2024 Kinetic theory of compressed neutral sheets. *Phys. Plasmas* (to be submitted).

Daughton, W. 2003 Electromagnetic properties of the lower-hybrid drift instability in a thin current sheet. *Phys. Plasmas* **10** (8), 3103–3119.

Daughton, W., Roytershteyn, V., Karimabadi, H., Yin, L., Albright, B.J., Bergen, B. & Bowers, K.J. 2011 Role of electron physics in the development of turbulent magnetic reconnection in collisionless plasmas. *Nature Phys*. **7** (7), 539–542.

Davidson, R.C. & Gladd, N.T. 1975 Anomalous transport properties associated with the lower-hybrid-drift instability. *Phys. Fluids* **18** (10), 1327–1335.

Denton, R.E., Sonnerup, B.U.Ö., Russell, C.T., Hasegawa, H., Phan, T.-D., Strangeway, R.J., Giles, B.L., Ergun, R.E., Lindqvist, P.-A., Torbert, R.B. *et al.* 2018 Determining L-M-N current sheet coordinates at the magnetopause from magnetospheric multiscale data. *J. Geophys. Res.: Space Phys*. **123**, 2274–2295.

Drake, J.F., Gladd, N.T. & Huba, J.D. 1981 Magnetic field diffusion and dissipation in reversed-field plasmas. *Phys. Fluids* **24** (1), 78–87.

DuBois, A.M., Crabtree, C., Ganguli, G., Malaspina, D.M. & Amatucci, W.E. 2022 MMS observations of a compressed current sheet: importance of the ambipolar electric field. *Phys. Rev. Lett*. **129** (10), 105101.

DuBois, A.M., Thomas, E. Jr., Amatucci, W.E. & Ganguli, G. 2013 Plasma response to a varying degree of stress. *Phys. Rev. Lett*. **111** (4), 145002.

DuBois, A.M., Thomas, E., Amatucci, W.E. & Ganguli, G. 2014 Density gradient effects on transverse shear driven lower hybrid waves. *Phys. Plasmas* **21** (6), 062117.

Egedal, J., Le, A. & Daughton, W. 2013 A review of pressure anisotropy caused by electron trapping in collisionless plasma, and its implications for magnetic reconnection. *Phys. Plasmas* **20** (6), 061201.

Egedal, J., Ng, J., Le, A., Daughton, W., Wetherton, B., Dorelli, J., Gershman, D. & Rager, A. 2019 Pressure tensor elements breaking the frozen-in law during reconnection in earth's magnetotail. *Phys. Rev. Lett*. **123**, 225101.

Fletcher, A.C., Crabtree, C., Ganguli, G., Malaspina, D., Tejero, E. & Chu, X. 2019 Kinetic equilibrium and stability analysis of dipolarization fronts. *J. Geophys. Res.: Space Phys*. **124**, 2010–2028.

Ganguli, G., Crabtree, C., Fletcher, A. & Amatucci, B. 2020 Behavior of compressed plasmas in magnetic fields. *Rev. Mod. Plasma Phys*. **4** (12), 1–89.

Ganguli, G., Crabtree, C., Fletcher, A.C., Tejero, E., Malaspina, D. & Cohen, I. 2018 Kinetic equilibrium of dipolarization fronts. *Sci. Rep*. **8**, 17186.

Ganguli, G., Keskinen, M.J., Romero, H., Heelis, R., Moore, T. & Pollock, C. 1994 Coupling of microprocesses and macroprocesses due to velocity shear: an application to the low-altitude ionosphere. *J. Geophys. Res*. **99** (A5), 8873–8889.

Ganguli, G., Lee, Y.C. & Palmadesso, P.J. 1988*a* Electron-ion hybrid mode due to transverse velocity shear. *Phys. Fluids* **31** (10), 2753.

Ganguli, G., Lee, Y.C. & Palmadesso, P.J. 1988*b* Kinetic theory for electrostatic waves due to transverse velocity shears. *Phys. Fluids* **31** (4), 823.

Graham, D.B., Khotyaintsev, Y.V., André, M., Vaivads, A., Divin, A., Drake, J.F., Norgren, C., Le Contel, O., Lindqvist, P.-A., Rager, A.C., *et al.* 2022 Direct observations of anomalous resistivity and diffusion in collisionless plasma. *Nature Commun*. **13** (1), 2954.

Greess, S., Egedal, J., Stanier, A., Daughton, W., Olson, J., Lê, A., Myers, R., Millet-Ayala, A., Clark, M., Wallace, J., *et al.* 2021 Laboratory verification of electron-scale reconnection regions modulated by a three-dimensional instability. *J. Geophys. Res.: Space Phys*. **126**, e2021JA029316.

GURNETT, D.A., ANDERSON, R.R., TSURUTANI, B.T., SMITH, E.J., PASCHMANN, G., HAERENDEL, G., BAME, S.J. & RUSSELL, C.T. 1979 Plasma wave turbulence at the magnetopause: observations from ISEE 1 and 2. *J. Geophys. Res*. **84** (A12), 7043.

HARRIS, E.G. 1962 On a plasma sheath separating regions of oppositely directed magnetic field. *Il Nuovo Cimento* **23** (1), 115–121.

HOSHINO, M., NISHIDA, A., MUKAI, T., SAITO, Y., YAMAMOTO, T. & KOKUBUN, S. 1996 Structure of plasma sheet in magnetotail: double-peaked electric current sheet. *J. Geophys. Res*. **101** (A11), 24775–24786.

HUBA, J.D. & GANGULI, G. 1983 Influence of magnetic shear on the lower-hybrid drift instability in finite β plasmas. *Phys. Fluids* **26** (1), 124–132.

HUBA, J.D., GLADD, N.T. & PAPADOPOULOS, K. 1978 Lower-hybrid-drift wave turbulence in the distant magnetotail. *J. Geophys. Res*. **83** (A11), 5217–5226.

HWANG, K.-J., GOLDSTEIN, M.L., MOORE, T.E., WALSH, B.M., BAISHEV, D.G., MOISEYEV, A.V., SHEVTSOV, B.M. & YUMOTO, K. 2014 A tailward moving current sheet normal magnetic field front followed by an earthward moving dipolarization front. *J. Geophys. Res.: Space Phys*. **119**, 5316–5327.

KHOTYAINTSEV, Y.V., GRAHAM, D.B., NORGREN, C. & VAIVADS, A. 2019 Collisionless magnetic reconnection and waves: progress review. *Front. Astron. Space Sci*. **6** (70), 1–20.

KOROVINSKIY, D.B., KIEHAS, S.A., PANOV, E.V., SEMENOV, V.S., ERKAEV, N.V., DIVIN, A.V. & KUBYSHKIN, I.V. 2021 The inertia-based model for reconstruction of the electron diffusion region. *J. Geophys. Res*. **126** (5).

KUMAR, T.A.S., MATTOO, S.K. & JHA, R. 2002 Plasma diffusion across inhomogeneous magnetic fields. *Phys. Plasmas* **9** (7), 2946.

LAPENTA, G., BERCHEM, J., ZHOU, M., WALKER, R.J., EL-ALAOUI, M., GOLDSTEIN, M.L., PATERSON, W.R., GILES, B.L., POLLOCK, C.J., RUSSELL, C.T., *et al.* 2017 On the origin of the crescent-shaped distributions observed by MMS at the magnetopause. *J. Geophys. Res.: Space Phys*. **122**, 2024–2039.

LE, A., EGEDAL, J., DAUGHTON, W., FOX, W. & KATZ, N. 2009 Equations of state for collisionless guide-field reconnection. *Phys. Rev. Lett*. **102** (8), 085001.

MAHAJAN, S.M. & HAZELTINE, R.D. 2000 Sheared-flow generalization of the Harris sheet. *Phys. Plasmas* **7** (4), 1287–1293.

MATSUBARA, A. & TANIKAWA, T. 2000 Anomalous cross-field transport of electrons driven by the electron-ion hybrid instability due to the velocity shear in a magnetized filamentary plasma. *Japan. J. Appl. Phys*. **39**, 4920–4932.

MCBRIDE, J.B., OTT, E., BORIS, J.P. & ORENS, J.H. 1972 Theory and simulation of turbulent heating by the modified two-stream instability. *Phys. Fluids* **15** (12), 2367–2382.

MCCOMAS, D.J., RUSSELL, C.T., ELPHIC, R.C. & BAME, S.J. 1986 The near-earth cross-tail current sheet: detailed ISEE 1 and 2 case studies. *J. Geophys. Res*. **91** (A4), 4287–4301.

NAKAMURA, R., BAUMJOHANN, W., ASANO, Y., RUNOV, A., BALOGH, A., OWEN, C.J., FAZAKERLEY, A.N., FUJIMOTO, M., KLECKER, B. & RÈME, H. 2006 Dynamics of thin current sheets associated with magnetotail reconnection. *J. Geophys. Res.: Space Phys*. **111**, A11206.

NORGREN, C., GRAHAM, D.B., KHOTYAINTSEV, Y.V., ANDRÉ, M., VAIVADS, A., HESSE, M., ERIKSSON, E., LINDQVIST, P.-A., LAVRAUD, B., BURCH, J., *et al.* 2018 Electron reconnection in the magnetopause current layer. *J. Geophys. Res.: Space Phys*. **123**, 9222–9238.

NORGREN, C., VAIVADS, A., KHOTYAINTSEV, Y.V. & ANDRÉ, M. 2012 Lower hybrid drift waves: space observations. *Phys. Rev. Lett*. **109**, 055001.

PETRUKOVICH, A.A., ARTEMYEV, A.V., MALOVA, H.V., POPOV, V.Y., NAKAMURA, R. & ZELENYI, L.M. 2011 Embedded current sheets in the Earth's magnetotail. *J. Geophys. Res*. **116**, A00I25.

PETRUKOVICH, A., ARTEMYEV, A., VASKO, I., NAKAMURA, R. & ZELENYI, L. 2015 Current sheets in the earth magnetotail: plasma and magnetic field structure with cluster project observations. *Space Sci. Rev*. **188**, 311–337.

POLLOCK, C., MOORE, T., JACQUES, A., BURCH, J., GLIESE, U., SAITO, Y., OMOTO, T., AVANOV, L., BARRIE, A., COFFEY, V., *et al.* 2016 Fast plasma investigation for magnetospheric multiscale. *Space Sci. Rev*. **199**, 331–406.

Rager, A.C., Dorelli, J.C., Gershman, D.J., Uritsky, V., Avanov, L.A., Torbert, R.B., Burch, J.L., Ergun, R.E., Egedal, J., Schiff, C., *et al.* 2018 Electron crescent distributions as a manifestation of diamagnetic drift in an electron-scale current sheet: magnetospheric multiscale observations using new 7.5 ms fast plasma investigation moments. *Geophys. Res. Lett*. **45**, 578–584.

Romero, H. & Ganguli, G. 1993 Nonlinear evolution of a strongly sheared cross-field plasma flow. *Phys. Fluids* B **5** (9), 3163–3181.

Runov, A., Sergeev, V.A., Nakamura, R., Baumjohann, W., Apatenkov, S., Asano, Y., Takada, T., Volwerk, M., Vörös, Z., Zhang, T.L., *et al.* 2006 Local structure of the magnetotail current sheet: 2001 Cluster observations. *Ann. Geophys*. **24** (1), 247–262.

Runov, A., Sergeev, V., Nakamura, R., Baumjohann, W., Vöros, Z., Volwerk, M., Asano, Y., Klecker, B., Rème, H. & Balogh, A. 2004 Properties of a bifurcated current sheet observed on 29 August 2001. *Ann. Geophys*. **22** (7), 2535–2540.

Russell, C.T., Anderson, B.J., Baumjohann, W., Bromund, K.R., Dearborn, D., Fischer, D., Le, G., Leinweber, H.K., Leneman, D., Magnes, W., *et al.* 2016 The magnetospheric multiscale magnetometers. *Space Sci. Rev*. **199**, 189–256.

Sanny, J., McPherron, R.L., Russell, C.T., Baker, D.N., Pulkkinen, T.I. & Nishida, A. 1994 Growth-phase thinning of the near-Earth current sheet during the CDAW 6 substorm. *J. Geophys. Res*. **99** (A4), 5805–5816.

Schindler, K. & Birn, J. 1993 On the cause of thin current sheets in the near-earth magnetotail and their possible significance for magnetospheric substorms. *J. Geophys. Res*. **98** (A9), 15477–15485.

Schindler, K. & Hesse, M. 2008 Formation of thin bifurcated current sheets by quasisteady compression. *Phys. Plasmas* **15**, 042902.

Schindler, K. & Hesse, M. 2010 Conditions for the formation of nongyrotropic current sheets in slowly evolving plasmas. *Phys. Plasmas* **17**, 082103.

Scudder, J. & Daughton, W. 2008 Illuminating electron diffusion regions of collisionless magnetic reconnection using electron agyrotropy. *J. Geophys. Res*. **113** (6), A06222.

Scudder, J.D. & Mozer, F.S. 2005 Electron demagnetization and collisionless magnetic reconnection in Be $\ll$1 plasmas. *Phys. Plasmas* **12** (9), 092903.

Sergeev, V.A., Mitchel, D.G., Russell, C.T. & Williams, D.J. 1993 Structure of the tail plasma/current sheet at -11RE and its changes in the course of a substorm. *J. Geophys. Res*. **98** (A10), 17345–17365.

Silin, I., Büchner, J. & Vaivads, A. 2005 Anomalous resistivity due to nonlinear lower-hybrid drift waves. *Phys. Plasmas* **12**, 062902.

Sitnov, M.I., Guzdar, P.N. & Swisdak, M. 2003 A model of the bifurcated current sheet. *Geophys. Res. Lett*. **30** (13), 1712.

Sitnov, M.I., Swisdak, M., Guzdar, P.N. & Runov, A. 2006 Structure and dynamics of a new class of thin current sheets. *J. Geophys. Res*. **111**, A08204.

Sonnerup, B.U. 1988 On the theory of steady state reconnection. *Comput. Phys. Commun*. **49** (1), 143–159.

Staniland, N.R., Dougherty, M.K., Masters, A. & Bunce, E.J. 2020 Determining the nominal thickness and variability of the magnetodisc current sheet at saturn. *J. Geophys. Res.: Space Phys*. **125** (5), e2020JA027794.

Takahashi, K. & Hones, E.W. Jr. 1988 ISEE 1 and 2 observations of ion distributions at the plasma sheet-tail lobe boundary. *J. Geophys. Res*. **93** (6), 8558–8582.

Torbert, R.B., Burch, J.L., Giles, B.L., Gershman, D., Pollock, C.J., Dorelli, J., Avanov, L., Argall, M.R., Shuster, J., Strangeway, R.J., *et al.* 2016*a* Estimates of terms in Ohm's law during an encounter with an electron diffusion region. *Geophys. Res. Lett*. **43**, 5918–5925.

Torbert, R.B., Russell, C.T., Magnes, W., Ergun, R.E., Lindqvist, P.-A., Le Contel, O., Vaith, H., Macri, J., Myers, S., Rau, D., *et al.* 2016*b* The FIELDS instrument suite on MMS: scientific objectives, measurements, and data products. *Space Sci. Rev*. **199**, 105–135.

Uzdensky, D.A., Loureiro, N.F. & Schekochihin, A.A. 2010 Fast magnetic reconnection in the plasmoid-dominated regime. *Phys. Rev. Lett*. **105**, 235002.

VAIVADS, A., ANDRÉ, M., BUCHERT, S.C., WAHLUND, J.E., FAZAKERLEY, A.N. & CORNILLEAU-WEHRLIN, N. 2004 Cluster observations of lower hybrid turbulence within thin layers at the magnetopause. *Geophys. Res. Lett*. **31**, L03804.

VALENTINI, F., TRÁVNÍČEK, P., CALIFANO, F., HELLINGER, P. & MANGENEY, A. 2007 A hybrid-Vlasov model based on the current advance method for the simulation of collisionless magnetized plasma. *J. Comput. Phys*. **225** (1), 753–770.

WALKER, D.N., AMATUCCI, W.E., GANGULI, G., ANTONIADES, J.A., BOWLES, J.H. & KOEPKE, M.E. 1997 Perpendicular ion heating by velocity-shear-driven waves. *Geophys. Res. Lett*. **24** (10), 1187–1190.

WILSON, L.B. III, BROSIUS, A.L., GOPALSWAMY, N., NIEVES-CHINCHILLA, T., SZABO, A., HURLEY, K., PHAN, T., KASPER, J.C., LUGAZ, N., RICHARDSON, I.G., *et al.* 2021 A quarter century of wind spacecraft discoveries. *Rev. Geophys*. **59** (2), 1–70.

XU, Y., FU, H.S., NORGREN, C., HWANG, K.J. & LIU, C.M. 2018 Formation of dipolarization fronts after current sheet thinning. *Phys. Plasmas* **25**, 072123.

YAMADA, M., KULSRUD, R. & JI, H. 2010 Magnetic reconnection. *Rev. Mod. Phys*. **82** (1), 603–664.

YOO, J., JI, J.-Y., AMBAT, M.V., WANG, S., JI, H., LO, J., LI, B., REN, Y., JARA-ALMONTE, J., CHEN, L.-J., *et al.* 2020 Lower hybrid drift waves during guide field reconnection. *Geophys. Res. Lett*. **47**, e2020GL087192.

https://doi.org/10.1017/S0022377823001447 Published online by Cambridge University Press